Cis-regulatory landscapes of the fat-tailed dunnart and mouse provide insights into the drivers of craniofacial heterochrony

Laura E. Cook[1,2,3*], Charles Y. Feigin[1], Andrew J. Pask[1 †], Irene Gallego Romero[1,2,4 *†]

1 School of Biosciences, University of Melbourne, Royal Parade, Parkville, Victoria, Australia

2 Melbourne Integrative Genomics, University of Melbourne, Royal Parade, Parkville, 3010 Victoria, Australia

3 Environmental Genomics & Systems Biology Division, Lawrence Berkeley National Laboratory, Berkeley, CA, USA

4 Center for Stem Cell Systems, University of Melbourne, Royal Parade, Parkville, 3010 Victoria, Australia

* To whom correspondence should be addressed: lecook@lbl.gov, irene.gallego@unimelb.edu.au

† These authors contributed equally

Abstract

Marsupials display accelerated development of the craniofacial region relative to the neurocranium when compared to placental mammals. This is thought to facilitate suckling by the highly altricial neonate after making the journey into the pouch. While *cis*-regulatory regions are considered to play a significant role in morphological evolution the face, the genetic mechanisms involved in craniofacial heterochrony among the major mammal lineages remain unclear. Here, we compared the *cis*-regulatory landscapes of the fat-tailed dunnart (*Sminthopsis crassicaudata*; Dasyuridae), a small marsupial amenable to laboratory husbandry, and mouse to gain insights into the basis of heterochrony. We compared patterns of the chromatin modifications, H3K4me3 and H3K27ac, between the dunnart and mouse during developmental stages when homologous craniofacial structures form each in species. We found that dunnart promoter- and enhancer- associated peaks at the time of birth in the dunnart broadly overlapped with all the stages of embryonic craniofacial development assessed in the mouse. However, dunnart-specific peaks were significantly enriched around genes whose mouse orthologs exhibit increased expression in the face over time. Moreover, genes displaying this temporal expression pattern were enriched for Gene Ontology terms related to ossification and skeletal development, processes that underlie development of the cranial muscles and bones of the face. This suggests a greater similarity between immediate postnatal chromatin landscape in the dunnart and late embryonic craniofacial development in the mouse. Using mouse-dunnart comparisons, we also discovered evidence of dunnart-specific peaks active near genes involved in the development of mechanosensory structures that may relate to the distinctive postnatal journey marsupial young take to the reach the pouch. This study characterised *cis*-regulatory elements driving craniofacial development in marsupials and their potential role in craniofacial heterochrony.

Introduction

The vertebrate head is a highly complex region of the body that plays a key role in an organism's ecology by centralizing numerous structures involved in diet, sensory perception and behaviour [1]. Consequently, evolution has modified craniofacial development across lineages, producing a wide array of head morphologies concomitant with the diverse niches that vertebrates occupy. Craniofacial diversity among the major mammal lineages in particular has long been of great interest, due to the striking differences in their developmental ontology.

In placental mammals, which are characterized by a long gestation and high maternal investment during pregnancy, a considerable degree of both orofacial and neurocranial development occurs *in utero* and thus experiences little functional constraint. By contrast, marsupials give birth to highly altricial young that must crawl to the teat, typically located within the maternal pouch, where they complete the remainder of their development *ex utero*. This unique reproductive method is though to have imposed strong pressures on the evolution and development of the limbs and head. In particular, marsupials show accelerated development of the nasal cavity, tongue, oral bones and musculature relative to the development of the posterior end of the body [2–5], and generally when compared to eutherian embryonic development [2, 3, 6]. Comparative morphometric studies have provided a wealth of evidence that this stark difference in craniofacial development has imposed different regimes of constraint on marsupial and placental mammals [2, 3, 6–9], with marsupials in particular showing significantly less interspecies variation in orofacial structures than placentals [9, 10]. In spite of these observations, the molecular mechanisms that underlie heterochrony between marsupial and placental craniofacial development remain poorly understood.

Cis-acting regulatory regions have been proposed to play a significant role in morphological divergence in the face, with a number of well-described enhancers that fine-tune face shape in mammals [11]. There is also some evidence of a role for regulatory regions in craniofacial heterochrony in marsupials. One recent study found a marsupial-specific region within a *Sox9* enhancer that drives early and broad expression in pre-migratory neural crest cell domains contributing to early migration of cranial neural crest cells relative to the mouse [12, 13]. However, no study has thus far attempted to compare the overall *cis*-regulatory landscape between marsupials and placental at developmentally comparable stages. Such surveys have the potential to provide functional insights into the loci controlling craniofacial heterochrony in mammals and consequently the causative evolutionary changes in the genome that have driven the divergent ontogenies of marsupials and placentals.

In recent years, the fat-tailed dunnart (*Sminthopsis crassicaudata*, hereafter referred to as the dunnart) has emerged as a powerful marsupial model species, comparable to the laboratory mouse in its laboratory husbandry and experimental tractability [14, 15]. Dunnarts are born after 13.5 days of gestation and craniofacial heterochrony in line with what has been reported in other marsupials is readily observable [2, 3, 6–9, 14], making this species an excellent system for comparative studies with placental models. Being one of the most altricial marsupials, the dunnart provides an ideal model in which to study the *cis*-regulatory landscape of heterochrony in craniofacial ossification in marsupials, as bony elements of the skeleton are not present until approximately 24 hours after birth, allowing ossification of the face to be studied *ex utero* in the pouch [14].

To investigate a potential role for *cis*-regulatory elements in this heterochrony, we used ChIP-sequencing on craniofacial tissue (fronto-nasal, mandibular and maxillary prominences) collected from new-born dunnart pouch young to first perform a detailed characterization of chromatin marks during early ossification and then to facilitate comparative analyses with the placental laboratory mouse. Our work provides valuable insights into genomic regions associated with cis-regulatory elements regulating craniofacial development in marsupials and their potential role in craniofacial heterochrony.

Results

Validation of ChIP-seq in dunnart craniofacial tissue

We performed ChIP-seq for H3K4me3 and H3K27ac in two biological replicate pools of dunnart pouch young that were < 24 hours old. Each replicate consisted of facial prominences from 25 animals. As the H3K4me3 and H3K27ac antibodies used in this work had not been previously used in marsupials, we first tested their reactivity in the dunnart using immunofluorescence and observed strong positive staining for both antibodies (Supplementary Figure 1a,b). Therefore, before sequencing, we validated the levels of enrichment in the ChIP libraries using qPCR and primers for sequences in the dunnart that were orthologous to the craniofacial enhancers mm428, mm387, mm423, hs466 and GH07J005561 and an enhancer active in the heart as a negative control, hs222. All primer sets were enriched as a percentage of the input control, and as expected no enrichment was observed in the rabbit and mouse mock IgG negative control samples (Supplementary Figure 1c). Although the dunnart ortholog of the human heart enhancer (hs222) was also enriched in both ChIP samples, this enhancer has only been tested at E11.5 in mouse embryos [16] and may have alternative roles at other stages in development or in different species.

Having validated the ability of our antibodies to enrich for dunnart chromatin marks, ChIP-seq libraries were sequenced to average depth of 57 million reads. Reads were mapped to a *de novo* assembly of the dunnart genome generated for this study, which we annotated using the publicly available high-quality genome assembly of the Tasmanian devil (mSarHar1.11 ;see Methods for additional details). After mapping and filtering, we retained an average of 43 million mapped reads per library. All samples had a non-redundant fraction (NRF) of between 0.76-0.85 [17]. Read coverage was highly correlated for replicates within each mark (Pearson's $r > 0.99$) and also between marks (Pearson's $r > 0.88$; Supplementary Figure 2a). Read coverage for replicate input controls was also correlated, but as expected due to enrichment for specific genomic regions in immunoprecipitation (IP) samples, there was no correlation in read coverage was observed between the input controls and IP samples (Pearson's r range = 0.03 to 0.08, Supplementary Figure 2a). Similarly, alignment BAM files for H3K4me3 and H3K27ac IP replicates show strong and specific enrichment indicated by a prominent and steep rise of the cumulative sum towards the highest rank, whereas input control alignment BAM files are roughly diagonal, highlighting even coverage across the genomic windows (Supplementary Figure 2b).

Defining craniofacial enhancer- and promoter- associated peaks in the dunnart

Peak calling with MACS2 ($q < 0.05$) identified 80,989 regions reproducibly enriched for H3K4me3 and 121,281 regions reproducibly enriched for H3K27ac in dunnart facial prominence tissue. Similar to previous studies [18–22], we found that H3K4me3 often (62% of all H3K4me3 peaks) co-occupied the genome with H3K27ac (Figure 1a) while 50% of H3K27ac-enriched regions were only associated with this single mark (Figure 1a). Active enhancers are generally enriched for H3K27ac [18, 23] while sites of transcription initiation (active promoters) can be identified as being marked by both H3K27ac and H3K4me3 [21, 22].

To categorise peaks are either promoter and enhancer -associated, we overlapped reproducible H3K4me3 and H3K27ac peaks. We initially defined promoter-associated peaks as those marked by only H3K4me3 or with > 50% of reciprocal peak length for H3K27ac and H3K4me3 peaks, and enhancer-associated peaks as those marked only by H3K27ac. We identified 66,802 promoter-associated peaks and 60,626 enhancer-associated peaks. Enhancer-associated peaks were located on average 77 kb from transcription start site (TSS), while promoter-associated peaks were located on average 106 kb from the nearest TSS, despite there being a greater number of peaks located < 1 kb from the TSS (1,008 enhancer-associated peaks versus 9,023 promoter-associated peaks; Figure 1b). This was an unexpected finding as a large fraction (0.41) of promoter-associated peaks were located > 3 kb from an annotated TSS. This may be a result of the incompleteness of the dunnart genome annotation or, as enhancers can also be associated with H3K4me3, may represent true biological signal [24].

To investigate this further, we first looked at the relationship between the number of peaks per gene and the distance to the next closest gene. After annotating peaks with the nearest gene call using ChIPseeker [25], 72% of genes had at least 1 promoter- or enhancer- associated peak, with 81 genes having more than 50 promoter-associated peaks (Supplementary Figure 3a). The number of promoter-associated peaks per gene was weakly positively correlated with distance to the next closest gene (Pearson's $r = 0.36$, $p < 2.2 \times 10^{-16}$), suggesting that this observation was partially due to the presence of unannotated transcripts between genes (Supplementary Figure 3b).

Enhancers can also be associated with H3K4me3. However, enrichment levels (peak intensity) tend to be lower than that of H3K27ac [24]. Hence, promoter-associated peaks located more than 3 kb from a known TSS may instead represent active enhancer regions [24]. To assess this we compared mean peak intensity in H3K4me3 peaks located greater than 3 kb from the nearest TSS, to H3K4me3 peaks located within 3 kb of the TSS. We found that H3K4me3 peaks located closer to the TSS had a stronger peak signal (mean = 46.10) than distal H3K4me3 peaks (mean = 6.95; Wilcoxon FDR-adjusted $p < 2.2 \times 10^{-16}$). This suggests that although some distal promoter-associated peaks may be due to missingness in the annotation, the majority likely represent peaks associated with enhancer regions. Although these issues are likely to also impact the annotation accuracy for enhancer-associated peaks, without additional transcript and epigenome data for the dunnart, it difficult to know which peak annotations are due to annotation quality and which represent true distal promoters.

Distance from TSS is frequently used to filter putative promoters from other elements; however, manually-selected distances are arbitrary and can lead to bias. Therefore, we used an unsupervised clustering approach to group promoter-associated peaks based on their distance to the nearest TSS. This analysis identified 3 clusters:

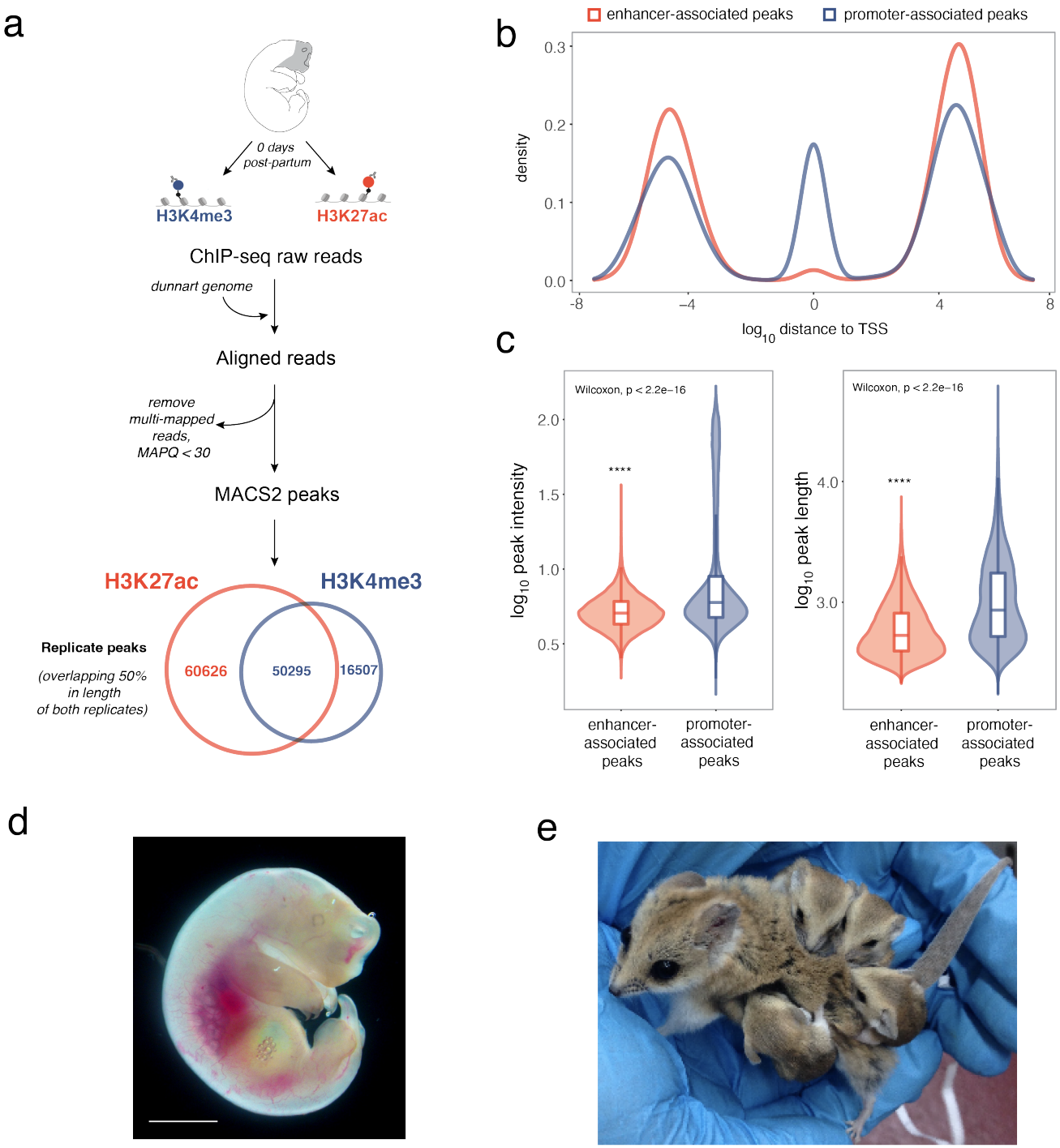

Figure 1: **Analysis workflow and quality control of H3K4me3 and H3K27ac peaks in the fat-tailed dunnart (*Sminthopsis crassicaudata*. a.** Short-read alignment and peak calling workflow and numbers of reproducible peaks identified for H3K27ac (orange), H3K4me3 (blue) for craniofacial tissue. **b.** Log_{10} distance to the nearest TSS for enhancer- (orange) and promoter- (blue) associated peaks. **c.** Log_{10} of peak intensity and peak length are represented as boxplots and violin plots for enhancer- (orange) and promoter- (blue) associated peaks. Peak intensities correspond to average fold enrichment values over total input DNA across biological replicates. **d.** Dunnart pouch young on the day of birth. Scale bar = 1mm. **e.** Adult female dunnart carrying four young.

upstream distal peaks (cluster 3, 31,285 peaks), downstream distal peaks (cluster 2, 22,863 peaks) and peaks centered on the TSS (cluster 1, 12,295 peaks; Supplementary Figure 4b). Peaks in cluster 1 (those closest to annotated TSS) had a higher GC and CpG island content than clusters 2 and 3 (Wilcoxon FDR-adjusted $p < 2.2 \times 10^{-16}$) and higher than enhancer-associated peaks (Wilcoxon FDR-adjusted $p < 2.2 \times 10^{-16}$), consistent with known features of mammalian promoters (Supplementary Figure 4e, f). Furthermore, cluster 1 peaks had a higher intensity (Supplementary Figure 4c) and length (Supplementary Figure 4d) when compared to clusters 2 and 3 (Wilcoxon FDR-adjusted $p < 2.2 \times 10^{-16}$) and compared to all enhancer-associated peaks and promoter-associated peaks (Wilcoxon FDR-adjusted $p < 2.2 \times 10^{-16}$). H3K4me3 ChIP-seq peak intensity has previously been correlated with transcriptional activity [26] and a higher peak intensity has also been observed in promoter-associated peaks in mammalian liver tissue [18]. We thus used cluster 1 (12295 peaks) to define a set of high-confidence promoter-associated peaks for all of the following analyses.

Candidate dunnart cis-regulatory elements are associated with craniofacial genes

Next, we asked what biological processes might be associated with promoter- and enhancer-associated peaks. To accomplish this, we first linked peaks to genes using ChIPseeker [25] in order to associate functional annotations of coding genes with the candidate cis-regulatory elements likely to regulate their expression. Next, we tested for GO term enrichment among genes associated with candidate promoters and candidate enhancers. We found that gene annotations for both enhancer- and promoter- associated peaks were enriched for 23% of the same GO terms, including cellular processes (protein localisation to plasma membrane, protein localisation to cell periphery, regulation of cell morphogenesis, positive regulation of cell migration) and development (axon development, camera-type eye development, muscle tissue development, striated muscle development).

By contrast, 42% of GO terms were uniquely enriched amongst genes assigned to promoter-associated peaks which were related to mRNA processing, transcription, mRNA stability, cell cycle, and mRNA degradation (Figure 2a; full results available as Supplementary File) and 36% of uniquely enriched GO terms for genes assigned to enhancer-associated peaks corresponded to processes indicative of early embryonic development (Figure 2a, Supplementary File).

Terms related to facial skeleton development were enriched amongst genes assigned to enhancer-associated peaks, including bone cell development, muscle cell development, secondary palate development, roof of mouth development and mesenchyme development, consistent with dunnart craniofacial morphology [14]. Enhancer-associated peaks active near important palate genes such as *Shh, Satb2, Mef2c, Snai2* and *Irf6* in the dunnart at birth may highlight potential regulatory mechanisms driving early palatal closure. In addition, terms related to development of the circulatory system, including regulation of vasculature development, circulatory system process and blood circulation were enriched amongst genes assigned to enhancer-associated peaks (for example, *Ace, Pdgfb, Gata4, Gata6, Vegfa*). This is consistent with observations that show the oral region of newborn dunnarts is highly vascularised, with blood vessels visible through their translucent skin at birth [14].

To gain further insight into dunnart gene regulation at this developmental stage, we scanned enhancer- and promoter- associated peaks for 440 known Homer vertebrate motifs and tested for enriched TFs [27]. Enhancer-

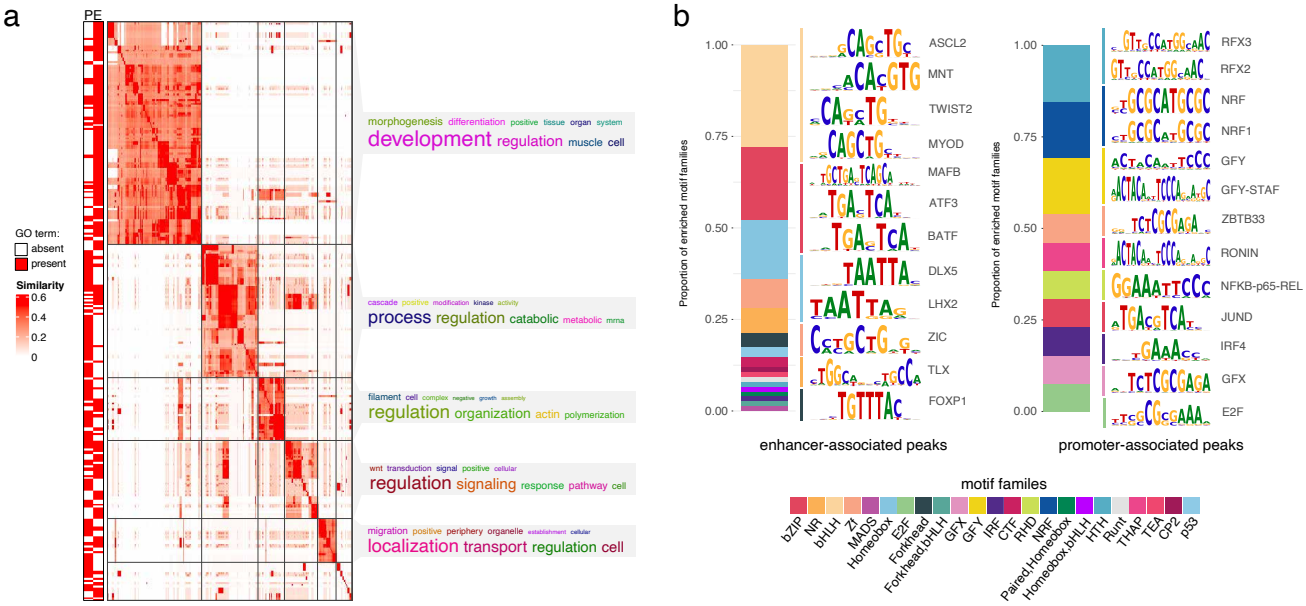

Figure 2: **Predicted functional enrichment for dunnart peaks a.** 304 significantly enriched GO terms clustered based on similarity of the terms. The function of the terms in each group are summarised by word clouds of the keywords. Each row represents a single GO term, rows marked by P were driven by genes linked to promoter-associated peaks, rows marked by E were driven by genes linked to enhancer-associated peaks. **b.** Enriched TF motifs for transcription factor families (HOMER). PWM logos for preferred binding motifs of TFs are shown. The letter size indicates the probability of a TF binding given the nucleotide composition.

associated peaks were significantly enriched for 170 TFs relative to a background set of random GC- and length matched sequences (FDR-corrected, $p < 0.01$), including those with known roles in differentiation of cranial neural crest cells (TWIST, HOXA2), skeletal morphogenesis (DLX5, CREB5, HOXA2), bone development (ATF3, RUNX), cranial nerve development (ATOH1) and/or facial mesenchyme development (LHX2, FOXP1, MAFB; Figure 2b, Supplementary Figure 5, Supplementary File). Consistent with the GO enrichment, transcription factor binding sites (TFBS) in promoter-associated peak sequences were dominated by transcriptional initiation regulatory sequences, with significant enrichment for 13 TFs (FDR-corrected, $p < 0.01$) including RFX3, RFX2, NRF, NRF1, GRY, ZBTB33, RONIN, JUND and GFX (Figure 2b, Supplementary Figure 5, Supplementary File).

Shifts in developmental timing of marsupial craniofacial regions are likely driven by recently evolved candidate enhancers

Previously, we defined the postnatal ossification series of the dunnart skull and characterized heterochrony between the orofacial and neurocranial regions [14]. Having now characterized the chromatin landscape of the dunnart's craniofacial/orofacial region, we next sought to compare it to that of a placental mammal which lacks the dunnart's distinctive craniofacial heterochrony. To do this, we took advantage of publicly available ChIP-seq data for H3K4me3 and H3K27ac generated by the mouse ENCODE consortium [17, 28] spanning multiple developmental time-points (E10.5-E15.5).

After peak calling as above, the number of H3K27ac and H3K4me3 peaks was fairly consistent across mouse

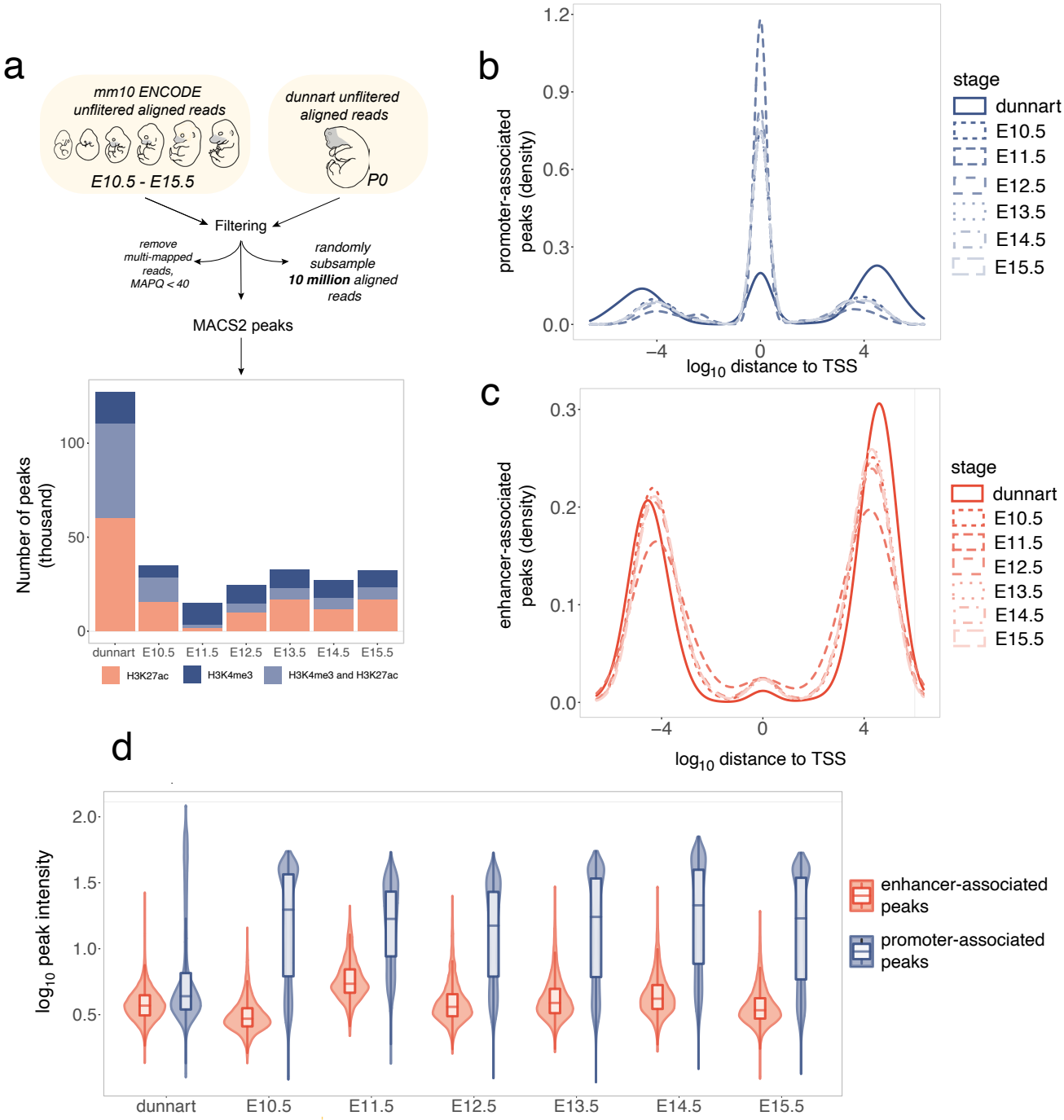

Figure 3: **Analysis workflow and features of H3K4me3 and H3K27ac peaks in dunnart and mouse.** **a.** Alignment filtering and peak calling workflow and number of reproducible peaks identified in the dunnart and mouse embryonic stages for H3K27ac and H3K4me3. Log_{10} of distance to the nearest TSS for **b.** enhancer- and **c.** promoter- associated peaks, **d.** Log_{10} peak intensity (measure of enrichment) for enhancer- (orange) and promoter- (blue) associated peaks.

embryonic stages (∼20-30,000 total peaks; Figure 3a). This number was significantly lower than the total number of peaks observed in the dunnart (∼150,000 peaks; Figure 3a). We investigated this further and found that the strength and specificity of enrichment differed between the mouse and dunnart datasets. Dunnart alignment BAM files for H3K4me3 and H3K27ac immunoprecipitation replicates show strong and specific enrichment (Supplementary Figure 2b); however, mouse alignment BAM files show a weaker enrichment with the immunoprecipitation samples for H3K27ac being closer to the input (Supplementary Figure 6c,d). This was also reflected in the similarity between mouse IPs and input controls based on read coverage, with correlation coefficients higher (H3K4me3, Pearson's r range = 0.17 to 0.32, Supplementary Figure 6b; H3K27ac, Pearson's r range = 0.39 to 0.64, Supplementary Figure 6a) than the corresponding dunnart values (Supplementary Figure 2a). Therefore, this is likely a technical confounder that may be responsible for the lower numbers of enriched regions called in the mouse, as peaks with lower enrichment signal might not be identified by the peak caller. This was consistent with the distribution of peak enrichment values in the dunnart and mouse for H3K4me3, with a lower mean peak enrichment value in the dunnart compared to all mouse stages (Kruskal-Wallis FDR-corrected $p = 6.7 \times 10^{-12}$; Figure 3d). However, this was not the case for peak enrichment values for H3K27ac peaks (Figure 3d), which generally have lower peak enrichment values than observed in H3K4me3 [18, 24].

As with the dunnart peaks, we filtered mouse peaks for reproducibility across biological replicates and categorised them as enhancer-associated (marked only by H3K27ac) or promoter-associated (marked by only H3K4me3 or > 50% of reciprocal peak length for H3K27ac and H3K4me3 overlapping peaks). Dunnart and mouse enhancer-associated peaks had a similar distribution of distances to the nearest TSS, with between 35-41% of peaks > 3kb from the nearest TSS (Figure 3c, Figure 4a,b) and between 34-40% of peaks in intronic regions (Figure 4a,b). Although the majority of mouse promoter-associated peaks were observed at the TSS, between 20-25% of peaks in the mouse data were located > 3kb from the closest TSS (Figure 4b), a lower fraction than observed in the dunnart (41%), potentially indicative of differences in enrichment and therefore the ability to call peaks with a weaker signal between the mouse and dunnart genomes. Thus, we filtered mouse peaks to retain only those within the same range of distances from a known TSS as the dunnart promoter-associated peaks ($\log_{10}$ = 2.3, Figure 4b). After filtering, the biological peak metrics were consistent between the dunnart and mouse, and between mouse stages, with a higher average percentage CpG (Wilcoxon $p < 2.2 \times 10^{-16}$) and GC content in the promoter-associated peaks (5.7% and 58% respectively) than enhancer-associated peaks (1.4% and 50%, respectively; Figure 4c). Mean $\log_{10}$ peak length and mean $\log_{10}$ peak intensity were also higher in the promoter-associated peaks (3.14 and 1.41) than enhancer-associated peaks (2.85 and 0.73, Wilcoxon $p < 2.2 \times 10^{-16}$) and this was consistent across species and embryonic stages used (Figure 4d).

Our previous work based on histological and microCT analyses proposed that D0 dunnart facial prominences correspond to that of the E11-E12 mouse embryo [14]. Therefore, we next compared active enhancer- and promoter- associated peaks between the dunnart and the six embryonic stages in the mouse in order to validate this observation and determine what stage in the mouse the regulatory landscape the D0 dunnart best corresponded to. Comparisons of non-coding DNA sequences across large evolutionary distances can be challenging due to the rapid sequence turnover [29]. After building dunnart-mm10 liftover chains (see Methods and

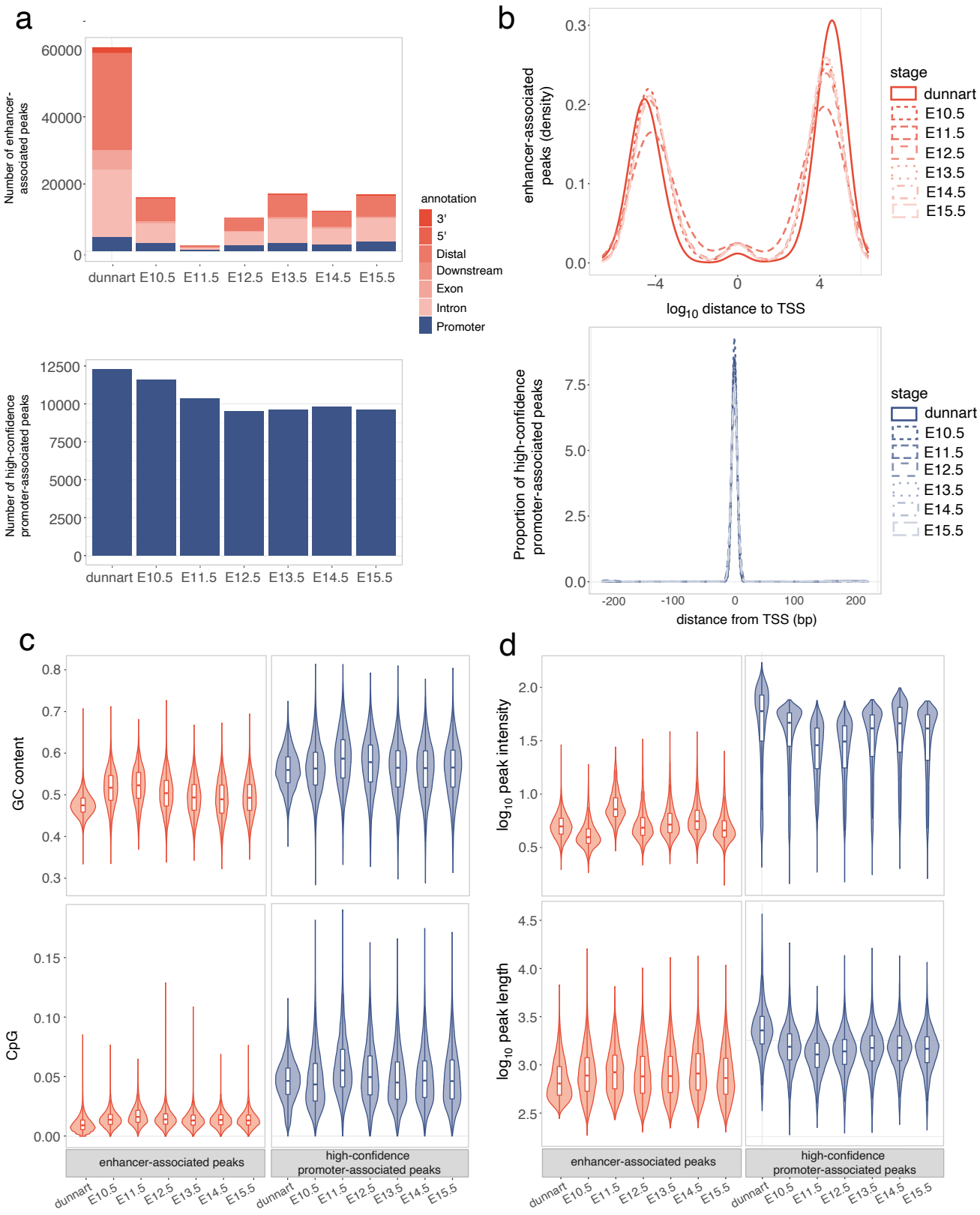

Figure 4: **Features of promoter-associated peaks and enhancer-associated peaks in the dunnart and mouse. a.** Genomic annotation for enhancer-associated (orange) and promoter-associated (blue) peaks. **b.** Log_{10} distance to the nearest TSS for enhancer-associated peaks (orange) and promoter-associated peaks (blue). **c.** CpG and GC content for enhancer- and promoter-associated peaks.**d.** Log_{10} peak intensity and $\log_{10}$ peak length for enhancer- and promoter- associated peaks.

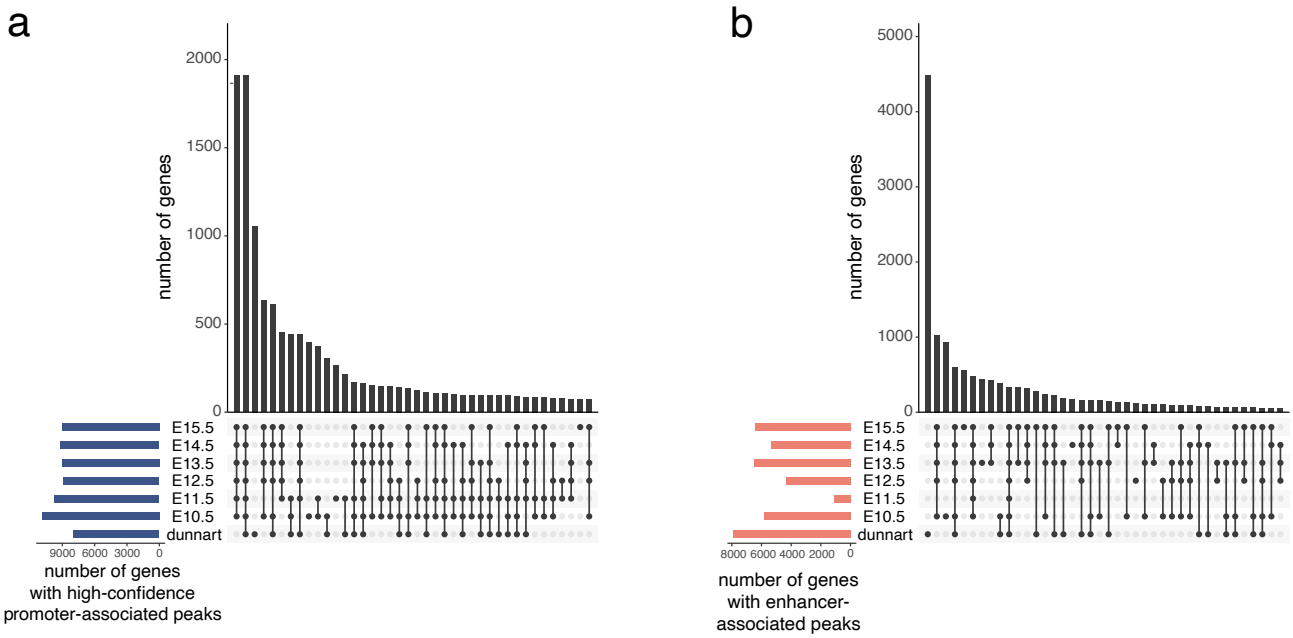

Figure 5: **Comparison of mouse and dunnart genes with enhancer- or promoter- associated peaks**. Intersections for genes with **a.** promoter-associated peaks and, **b.** enhancer-associated peaks.

Supplementary Information) we found that between 0.74-6.77% of enhancer-associated peaks out of all alignable enhancer-associated peaks were present in both mouse and dunnart (Supplementary Table 13b). In contrast, between 45-57% of alignable promoter-associated peaks were present in mouse and dunnart (Supplementary Table 13a). Although this is a small fraction of the total peaks (∼8% for promoter-associated peaks and ∼0.5 % of enhancer-associated peaks (Supplementary Table 13), it suggests that, consistent with the literature [18], promoter regions are more stable over large evolutionary distances and that shifts in developmental timing of craniofacial marsupial may be more likely to be driven by recently evolved enhancer regions in marsupials.

Genes associated with candidate dunnart CREs are enriched for a cluster of genes upregulated during ossification of the orofacial region in the mouse

Given the large evolutionary distance between the mouse and dunnart and low recovery of conserved peaks, we performed a comparison between species at the gene level, by comparing genes assigned to peaks between the dunnart and mouse. The number of genes that intersect can provide an idea of the similarities in genes and pathways regulated across a large subset of the total peak dataset.

The largest intersection size in genes with promoter-associated peaks was between the six mouse embryonic stages (1,910 genes; 21.2%) and between the dunnart all six embryonic mouse stages (1,908 genes, 21.2%; Figure 5a). We found the dunnart had 1,055 genes with promoter-associated peaks that did not intersect with any embryonic stage in the mouse, suggesting there is a unique set of genes regulated in the dunnart at this stage of craniofacial development (Figure 5a).

Overlap between enhancer-associated peaks was more restricted, with 4,483 nearest gene calls (56%) being unique to the dunnart at D0 (Figure 5b). This is exacerbated by the very small number of peaks detected at E11.5 (7510 peaks; Supplementary Table 9), a missingness likely to represent technical, rather than biological

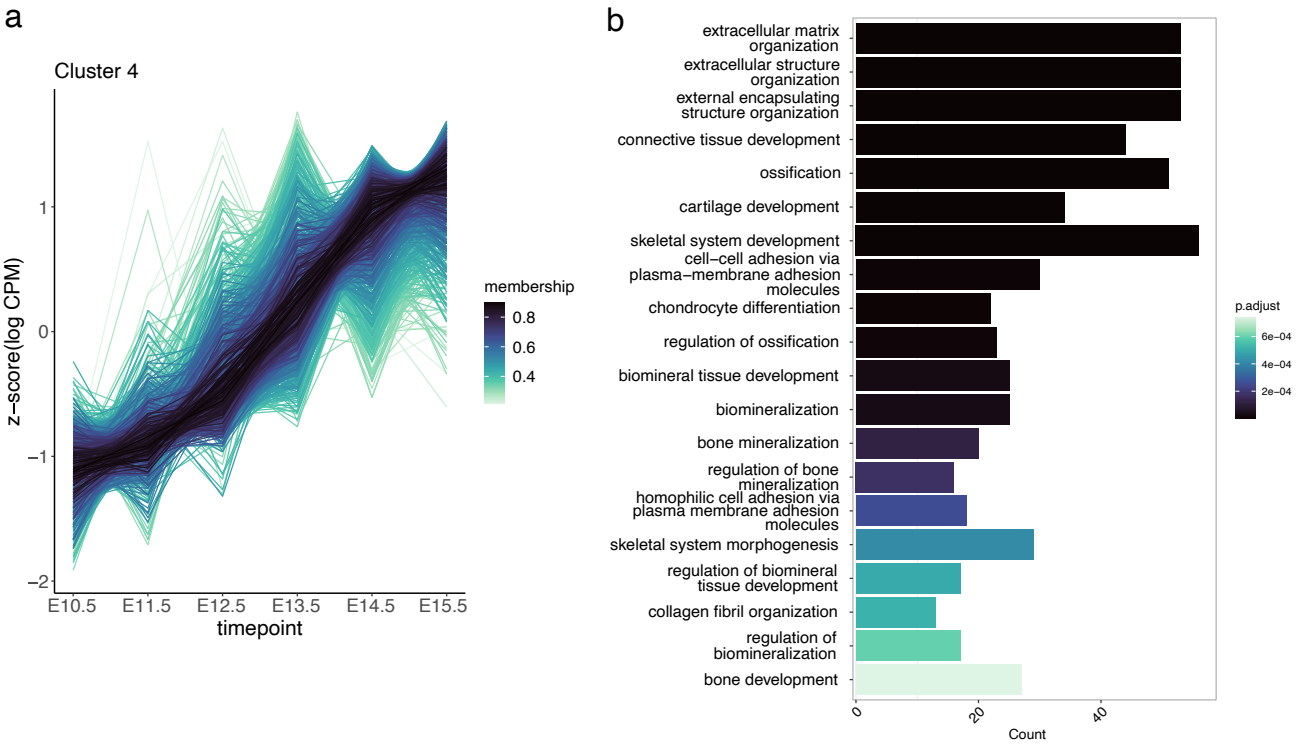

Figure 6: **Clustering genes by temporal expression dynamics. a.** Genes near promoter-associated peaks are significantly enriched in cluster 2. **b.** GO enrichment for biological processes in cluster 2. **c.** Genes near enhancer-associated peaks are significantly enriched in cluster 4. **d.** GO enrichment for biological processes in cluster 4

signal. 592 genes (7.4%) with enhancer-associated peaks are common across the dunnart and E10.5, E12.5-E15.5, and an additional 338 genes (4.2%, but 30.7% of all genes with E11.5 peaks) found in the dunnart and all five embryonic stages in the mouse. The mouse stages with the largest private overlap in genes with the dunnart were E10.5 and E15.5, with 379 (4.73%) and 277 (3.46%) genes respectively (Figure 5b).

From this, it appeared that genes with assigned promoter-associated peaks were shared across mouse embryonic stages and between species. Despite differences in intersection sizes between the dunnart and mouse embryonic stages, we found that the top enriched terms for biological processes were largely shared across dunnart and mouse (Supplementary Figure 7a).

On the basis of the above, there was no single developmental stage in mouse with clear equivalence to D0 in the dunnart. This is not unexpected, given the shifts in developmental timing of the craniofacial structures in the dunnart relative to the mouse. To further contextualise these patterns, we retrieved mouse gene expression data from embryonic facial prominence tissue collected from E10.5 to E15.5 in the mouse ENCODE database [17, 28], and incorporated this into our comparative analyses. Across the entire dataset, 15,348 genes had log2CPM > 1) across biological replicates for at least one stage in embryonic development (Supplementary File). We examined temporal gene expression patterns across this dataset by using the TCseq package [30]. Specifically, we used C-means clustering to identify five specific groups with differing temporal gene expression patterns throughout embryonic development (Supplementary Figure 8, Supplementary File). Each of these groups displayed distinct temporal expression patterns that likely reflect biological processes occurring during development of the embryonic facial prominences (Supplementary Figure 8, Supplementary File).

Finally, we compared the lists of dunnart genes with promoter-associated peaks and enhancer-associated peaks to the distinct temporal gene expression clusters. Of all five clusters, dunnart genes with either promoter-associated and enhancer-associated peaks were significantly over-represented only amongst those genes in cluster 2 (Hypergeometric test, genes with promoter-associated peaks: $p.adjusted = 0.00384$, gene with enhancer-associated peaks: $p.adjusted = 0.00593$; Figure 6a, all other tests $p.adjusted > 0.05$). This cluster consisted of genes that are downregulated in early mouse embryonic development (E10.5) with linear increase in expression from E11.5 to E15.5. Genes in this cluster were significantly enriched for GO terms involved in the development of the skeletal system including bone mineralisation, muscle system process, ossification, cartilage development, regulation of ossification and skeleton system morphogenesis (Figure 6b). This included critical craniofacial developmental genes such as the master bone growth regulator, *Runx2*, as well as *Bmp6*, *Dmrt2*, *Mef2c*, *Fgf2*, *Sp7/Osx*. Enrichment for peaks predicted to regulate key ossification genes is consistent with ossification patterns observed in the dunnart. The first appearance of bone in the orofacial region and limbs at approximately 1 day post-birth [14] in the dunnart and from E14.5 in mouse. Taken together, the results of our analyses provide clear candidates involved in craniofacial development in the fat-tailed dunnart. Additionally, the putative cis-regulatory elements described here are likely to play an important role in the craniofacial heterochrony that is characteristic of marsupials.

Discussion

Marsupials display accelerated development of the craniofacial region relative to the differentiation of the neurocranium when compared to placental mammals [3, 6]. Despite increasing descriptions of craniofacial enhancers in model species [11, 31], the genetic drivers of craniofacial heterochrony remain largely unexplored. In this study, we examined the similarities and differences in genomic regions marked by H3K4me3 and H3K27ac between the dunnart and mouse during early craniofacial development. This is the first description of genome-wide craniofacial regulatory elements in a marsupial with 60,626 enhancer-associated peaks and 12,295 promoter-associated peaks described.

The biological processes enriched for genes with dunnart enhancer-associated peaks were also consistent with features that are accelerated or unique to the dunnart and marsupials more broadly. In particular, we observed a significant excess of genes with enhancer-associated peaks involved in secondary palate development and roof of mouth development, a trait that is accelerated in the dunnart compared to eutherian mammals [32–34]. Enhancer-associated peaks active near important palate genes such as *Shh, Satb2, Mef2c, Snai2 and Irf6* in the dunnart at birth may highlight potential regulatory mechanisms driving early palatal closure. In addition, the enrichment for peaks predicted to regulate key genes involved in circulatory system processes and blood circulation (such as *Ace, Pdgfb, Gata4, Gata6, Vegfa*) are consistent with the vascularization needed to support the dynamic and rapid development of tissue in newborn dunnarts [14]. Enrichment for these terms may also be related to the gas exchange process in newborn dunnarts. Newborn dasyurids have canalicular stage lungs (equivalent to the human foetus at approximately 17 weeks of gestation and to the mouse embryo at E16.5) and

instead undergo cutaneous gas exchange with a high capillary volume density and a short skin diffusion barrier [35–38].

Despite 160 million years divergence and significant difference in non-coding regions of the genome, 8% of dunnart promoter peaks could be aligned to the mouse genome. Of those that could be aligned, we found that between 45-57% of alignable promoter-associated peaks had a corresponding enriched peak in the mouse (Supplementary Table 13a) Genes near promoter-associated peaks were largely common between species and across mouse embryonic stages (Figure 5b). In comparison, much of the signal coming from majority of enhancer-associated peaks were dunnart-specific. Of the dunnart enhancer peaks that could be aligned to the mouse genome, only 0.74-6.77% had a corresponding peak in the mouse ChIP-seq data. Additionally, the majority of genes near enhancer-associated peaks (77%) were species-specific and of those that overlapped in the dunnart and mouse, 40% were stage-specific (Figure 5b). This is consistent with the [18, 39–41], suggestion that promoter regions are more stable over large evolutionary distances and that shifts in developmental timing of craniofacial regions in marsupials may be more likely to be driven by recently evolved enhancer regions.

Genes near promoter-associated peaks were often enriched for ubiquitous cellular processes (Supplementary Figure 7, Supplementary File), while genes near enhancer-associated peaks were enriched for terms associated with developmental processes undergoing in the face during this developmental window including "ossification", "cartilage development", "connective tissue development", "mesenchyme development" and "skeletal system development". Genes near both promoter- and enhancer- associated peaks were enriched for the Wnt-signalling pathway. Likewise, dunnart ChIP-seq peaks were significantly enriched around genes that exhibit increased expression from E10.5 to E15.5 in mice. Genes displaying the aforementioned temporal expression pattern were enriched for GO terms related to ossification and skeletal development, processes that underlie development of the cranial muscles and bones of the face. This included critical craniofacial developmental genes such as the master bone growth regulator, *Runx2*, as well as *Bmp6*, *Dmrt2*, *Mef2c*, *Fgf2*, *Sp7/Osx*. *Runx2*[42–44], *Bmp6*[45, 46] and *Mef2c*[47] have previously been suggested to contribute to vertebrate craniofacial diversity. Early development of the oral region and onset of ossification observed in our previous work in the dunnart [14] could be driven by cis-regulatory elements targeting these genes.

While the top enriched GO terms were generally shared for genes with enhancer-associated peaks in mouse and dunnart, one GO term, "sensory system development" was enriched in the dunnart but not in any of the mouse embryonic stages. This was driven by genes such as *Tmem132e, Bmp4/7, Ntrk3, Shh, Isl1, Notch2, Fgfr2, Bdnf, Ctnnb1 and Lmx1b*, which are known to be involved in development of the mammalian mechanosensory structures [48–51]. Newborn marsupial young require developed sensory systems to respond to the cues that guide them to the teat inside the mother's pouch, with the nasal-oral region making regular contact with the mother's belly during the crawl to the pouch [52–54]. The snout epidermis of newborn marsupials has been shown to be innervated with presence of mature Merkel cells with connected nerve terminals [55]. When pressure is applied to the innervated snout this induces electromyographic responses from the triceps muscle in both forelimbs, suggesting that the journey to the pouch may be aided by the influence of facial mechanosensation on forelimb movement [52]. Merkel cells develop much later in the mouse during embryonic development (E16.5 - P0) [48],

and is likely why peaks near genes involved in the development of these cell types were not observed in the mouse ChIP-seq data. This is also consistent with the gene expression time series data in the mouse from E10.5-E15.5, with key Merkel cell developmental genes [48] either lowly expressed (*Shh and Ntrk3*) or not expressed during this developmental window in the face (*Bmp7, Notch2, Fgfr2, Bdnf, Lmbx1b, Ctnnb1*; Supplementary File). This highlights a previously unstudied aspect of the craniofacial heterochrony observed in marsupials and eutherian mammals, related to the potentially critical role of the epidermis in the marsupial journey to the pouch.

The amount of overlap we observed in the mouse and dunnart genes near peaks is striking, given the significant differences in experimental methods between the datasets we have analysed, and highlights core conserved gene regulatory networks during mammalian development. The mouse ChIP-seq data was generated with a different experimental protocol and sequenced using a single-end configuration, at a lower sequencing depth than the dunnart data we report. Even with library depth normalisation, stronger enrichment was observed in the dunnart ChIP-seq data than in the mouse data (see Supplementary Figure 2 and Supplementary Figure 6). Second, the dunnart is a draft genome assembly without a *de novo* transcriptome. We used liftOff [56] to import the Refseq annotation from the Tasmanian devil, which is itself incomplete and not of the same quality as that available for the mouse genome. This was evident when comparing orthologous Ensembl genes, where 40% of annotated peaks were lost as there was no associated Ensembl ID in the conversion table. Third, the mouse and dunnart peaks described here are connected to genes solely on the basis of genomic proximity and in the absence of expression data from the dunnart, we cannot conclude that the peaks described here contribute to transcriptional output. The annotation quality in the dunnart could have also led to inaccurate gene-peak pairing. Furthermore, the craniofacial tissue assayed here is a mix of cell and tissue types derived from different embryological origins and may represent craniofacial structures that are accelerated and others that are delayed.

Based on previous observations [5], we hypothesised that the dunnart craniofacial structures on the day of birth would be approximately similar to E11.5 – E12 in the mouse. However, we found that genes near ChIP-seq peaks overlap to some extent with all mouse embryonic stages we considered, and it was not clear that the dunnart D0 had a single clear corresponding stage in the mouse. This suggests that regulatory pathways active sequentially during development of the facial prominences in mice might instead operate concurrently in the dunnart as a result of the shorter *in utero* gestation period and the functional demands on the oral region for suckling post-birth. Using mouse-dunnart comparisons, we also discovered evidence of dunnart peaks active near genes involved in the development of mechanosensory structures that may relate to the unique journey taken to the pouch in marsupials. Additionally, in undertaking this study we have developed fundamental genomic resources for this novel model species including a *de novo* genome assembly, a reference annotation and liftOver chains to the mouse genome (mm10). These will be valuable resources for work continuing to define areas of the genome driving the evolution of complex traits and mechanisms underpinning heterochrony and, more broadly, marsupial and mammalian development.

Methods

Tissue collection

All animal procedures, including laboratory breeding, were conducted in accordance with the current Australian Code for the Care and Use of Animals for Scientific Purposes[57] and were approved by The University of Melbourne Animal Ethics Committee (AEC: 1513686.2) and with the appropriate Wildlife Permit (number 10008652) from the Department of Environment, Land, Water and Planning. Animals were housed in a breeding colony in the School of BioSciences, The University of Melbourne. For details on animal husbandry and collection of dunnart pouch young refer to [5]. Details of pouch young used in this study are presented in Supplementary Table 1. After removal of pouch young from the teat, young were killed by decapitation and craniofacial tissue dissected using insulin needles (Becton Dickinson). The tongue, neural tube and eye primordia were removed to limit tissue collected to the facial prominences. Specifically, the mandibular, maxillary and fronto-nasal prominences were collected and snap frozen in liquid nitrogen. All pouch young were determined to be <24 hours old but to account for variability in time since birth we scored pouch young based on head shape. Immediately after birth the dunnart has a flat neurocranium that by approximately 1 day after birth has begun to round (see [5] for more details). We combined craniofacial tissue from 50 pouch young into two replicates ensuring that sex, head shape, and parentage were accounted for (Supplementary Table 1).

Immunofluorescence

We assessed the reactivity of the ChIP antibodies in the dunnart using immunostaining on dunnart head sections. Frontal head sections (7 μm thick) on superfrost slides (Platinum Pro, Grale) were deparaffinised and re-hydrated according to standard methods [58], followed by antigen retrieval using pH 8.8 unmasking solution (Vector) at 99°C for 30 minutes. We then incubated the sections with either rabbit anti-H3K4me3 primary antibody (1:500 dilution; Abcam ab8580) or rabbit anti-H3K27ac primary antibody (1:500, Abcam ab4729). Sections were then incubated with Alexa Fluor 555 donkey anti-rabbit antibody (1:500 dilution; Abcam in 10% horse serum in PBS with 0.1% Triton X-100, (Sigma)). All sections were counterstained with 300 nM DAPI to visualise cell nuclei. We observed no staining in the negative controls (no primary antibody). Images were captured using fluorescence microscopy (BX51 Microscope and DP70 Camera; Olympus) and processed in ImageJ v 2.0.0 [59].

Chromatin immunoprecipitation

Chromatin immunoprecipitation (ChIP) was performed using the MAGnify^{TM} Chromatin Immunoprecipitation System (Thermo Fisher, 492024) according to manufacturer's instructions. Briefly, frozen dunnart tissue samples (see Supplementary Table 1) were diced quickly with two razor blades in cold dPBS (Gibco) followed by crosslinking in 1% formaldehyde solution (Sigma) for 10 minutes. We then added 0.125 M glycine and incubated for 5 minutes at room temperature to neutralize the formaldehyde. Chromatin was fragmented to 300 bp average size by sonication on a Covaris S2 using the following parameters: duty cycle = 5%, intensity = 2, cycles per burst = 200, cycle time = 60 seconds, cycles = 10, temperature = 4°C, power mode = frequency sweeping, degassing

mode = continuous. In each ChIP experiment, we used sheared chromatin from each replicate for immunoprecipitation with antibodies against H3K4me3 (Abcam ab8580) and H3K27ac (Abcam ab4729). An input control was included for each replicate. DNA was purified according to kit instructions using a DynaMag^{TM}-PCR Magnet (Thermo Fisher).

ChIP-qPCR validation

We assessed the success of the immunoprecipitation in dunnart craniofacial tissues by performing qPCR for primers designed to amplify genomic regions expected to occupied by H3K4me3 and/or H3K27ac (based on mouse and human enhancers active in facial regions of E11.5 mice in VISTA enhancer [16] and GeneHancer [60], Supplementary Table 2). We also designed primers that amplify regions we predicted would be unoccupied by these histone modifications (enhancers active in heart tissue of E11.5 mice in VISTA enhancer browser[16], Supplementary Table 2). qPCR using SYBR Green Supermix (Bio-Rad Laboratories) was performed in triplicate on a QuantStudio™ 5 System (Thermo Fisher) as per manufacturers instructions (primers listed in Supplementary Table 2). The cycling conditions were as follows: one cycle of 95°C for 15 s, followed by 40 cycles of 95°C for 15 s, 57°C for 30 s and 72°C for 30 seconds. A dissociation curve was also generated for each primer pair. No-template controls were included in triplicate on each plate as a negative control. Regions expected to be enriched in the test sample were quantified by expressing the test sample as a fold change relative to a control sample (no antibody control).

ChIP sequencing

Illumina sequencing libraries were prepared from ChIP-enriched DNA by GENEWIZ (Suzhou, China). Libraries were constructed following the manufacturer's protocol (NEBNext UltraTMII DNA Library Prep Kit for Illumina). For each sample, a minimum of 10 ng of ChIP product was used and libraries were multiplexed and sequenced on an Illumina HiSeq 4000 instrument according to manufacturers instructions (Illumina, San Diego, CA, USA). Sequencing was carried out using a 2x150 paired-end configuration to an average depth of 57 million read pairs per sample.

Genome assembly and annotation

Previously there was no fat-tailed dunnart genome available to map ChIP-seq reads against. In order to generate a genome for dunnart, tissue was collected and four sequencing libraries were prepared following 120 previous methods [61]. Four libraries were generated to improve molecular complexity and genome representation of input DNA. These libraries were then sequenced using the following technologies: Illumina X Ten 2x150 bp, PacBio Sequel I CLR, ONT PromethION and ONT GridION (Supplementary Table 3).

Quality trimming and residual adaptor removal from dunnart Illumina libraries (Library 1) was performed using trimmomatic v0.38 [62] (options: `PE SLIDINGWINDOW 5:20, MINLEN 75, AVGQUAL 30`). Contigs were assembled using 200 Gb of PacBio CLR subreads (Library 2) using Flye v2.7 [63] with options: `{iterations`

4 {trestle {pacbio-raw {genome-size 3.0g. Removal of redundant contigs and two rounds of short-read and long-read scaffolding were performed using Redundans 0.14a [64] with options: `--nogapclosing --limit 1.0`. Inputs for redundans scaffolding were short-insert paired-end reads (Library 1) and 6.5 gigabases of Oxford Nanotechnology reads corresponding to 2 libraries (Library 3 and Library 4). Scaffolds then underwent two rounds of polishing to improve base quality using Pilon v1.23 [65] with Illumina Library 1 as input and with options: `--vcf --diploid --chunksize 10000000 --fix snps,indexls,gaps --minqual 15`. The resulting genome assembly had a total size of 2.84 Gb and an N50 length of 23 megabases (Mb). See Supplementary Table 3 for descriptions of all input libraries used in the assembly. We used BUSCO v5.2.2 to assess genome completeness (v3.0.2, -l mammalia_odb10 -m genome). BUSCO gene recovery was 89.9% for complete orthologs in the mammalia_odb10 lineage dataset which includes 9226 BUSCOs. Together, these metrics indicate that the assembly is of comparable completeness and contiguity to other recently-published marsupial genomes [66–72] and therefore represents an excellent resource for downstream functional genomic experiments. The resulting *de novo* assembly with a resulting scaffold N50 of 23 megabase pairs (Mb) and a total size of 2.84 gigabase pairs (Gb) making it comparable to other marsupial genomes [67–70]. The GC content of the *de novo* contigs in the dunnart (∼36.25%), was similar to other marsupial species (Tasmanian devil; 36.4% [69], thylacine; ∼36% [67], wallaby; 34-38.8% [68], opossum; 37.8% [70]), woylie; 38.6% [71] and the brown antechinus; 36.2% [72].

Gene annotations from the high-quality genome assembly of the Tasmanian devil (Sarcophilus harrisii, GCF_902635505.1 - mSarHar1.11), which has a divergence time with the dunnart of approximately 40 million years, were accessed from NCBI and then lifted over to dunnart scaffolds using the program liftoff v1.0 [56] with option `--d 4`.

Whole genome alignment

To compute pairwise genome alignments between the mouse and dunnart, we used the mouse mm10 assembly as the reference. We first built pairwise alignments using Lastz and `axtChain` to generate co-linear alignment chains [73], using the previously described Lastz parameters for vertebrates, `K = 2400 L = 3000 Y = 3400, H = 200` with the HoxD55 scoring matrix [74]. After building chains, `patchChain` [74] was applied to extract all the unaligned loci and create local alignment jobs for each one. The new local alignments were combined with the original local alignments for an improved set of chains. We then applied `chainCleaner` [75] with the parameters `-LRfoldThreshold = 2.5 -doPairs -LRfoldThresholdPairs = 10 -maxPairDistance = 10000 -maxSuspectScore = 100000 -minBrokenChainScore = 75000` to improve the specificity of the alignment. After generating an improved set of chains, we applied `chainPreNet`, `chainNet` and `netChainSubset` to filter, produce the alignment nets and create a single chain file using only the chains that appear in the alignment nets [73]. Alignment nets are a hierarchical collection of the chains that attempt to capture orthologous alignments [73]. Chain fragments were joined using `chainStitchId` and dunnart to mouse chains generated using `chainSwap` [73] (Supplementary File). For quality control, maf files were generated using `netToAxt` and `axtToMaf` [73]. Block counts, block lengths and pairwise divergence in the alignments were assessed using `MafFilter` [76].

ChIP sequencing quality assessment

First, we assessed the raw sequencing read quality using FastQC v0.11.9 [77]. Raw data were processed by adapter trimming and low quality read removal using Cutadapt v1.9.1 [78] [-q 20 -a AGATCGGAAGAGCACACGTCTGAACTCCAGTCA -A AGATCGGAAGAGCGTCGTGTAGGGAAAGAGTGT –max-n 0.10 -m 75]. ChIP sequencing statistics for raw reads and trimmed reads are described in Supplementary Table 4.

ChIP sequence alignment, peak calling and annotation

Sequencing reads were aligned to the dunnart genome with Bowtie2 v.2.3.5.1 [79] (parameters: `-q -X 2000 --very-sensitive`). Unfiltered aligned reads from ChIP-seq experiments performed using mouse embryonic facial prominence for E10.5, E11.5, E12.5, E13.5, E14.5 and E15.5 were downloaded from ENCODE.org [17, 28, 80] (accession details described in Supplementary Table 5). For both dunnart and mouse aligned reads, low-quality and unpaired reads were removed using Samtools v.1.9 [81] (parameters: `-q 30 -f 2`) and duplicate reads removed by the MarkDuplicates tool from picard v.2.23.1 (http://broadinstitute.github.io/picard/). Mapping statistics and library complexity for dunnart and mouse reads are described in Supplementary Table 6 and Supplementary Table 7, respectively. Effective genome size for the dunnart was calculated using the `unique-kmers.py` script from khmer v.2.0 [82]. Peaks were called on the dunnart-aligned reads using MACS2 v.2.1.1 [83] (parameter: `-f BAMPE`) and the mouse aligned reads using MACS2 v.2.1.1 with default parameters for mm10, using total DNA input as control and retaining all statistically significant enrichment regions (FDR-corrected $P < 0.01$). Reproducible consensus peaks for biological replicates within a species were determined using the ENCODE3 `overlap_peaks.py` script [17, 28]. Enriched regions were considered reproducible when they overlapped in two biological replicates within a species by a minimum of 50% of their length using bedtools intersect v2.29.2 [84]. Peak-calling statistics for dunnart and mouse are described in Supplementary Table 8 and Supplementary Table 9, respectively. Similar to [18], we overlapped H3K4me3 and H3K27ac reproducible peaks to determine promoter-associated peaks (marked by only H3K4me3 or both H3K4me3 and H3K27ac) and enhancer-associated peaks (marked only by H3K27ac). H3K4me3 and H3K27ac reproducible peaks were overlapped to determine genomic regions enriched for H3K4me3, H3K27ac or both marks using bedtools intersect v2.29.2 [84]. Double-marked H3K4me3 and H3K27ac elements were defined as regions reproducibly marked by H3K4me3 and H3K27ac and overlapping by a minimum 50% of their reciprocal length and were merged with bedtools v2.29.2 [84]. Dunnart peak calls from the entire data set can be found in the Supplementary File . Mouse and dunnart peaks called on 10 million aligned reads can be found in the Supplementary File .

Gene annotation and Gene Ontology analyses

Gene annotations lifted over from the Tasmanian devil annotation were associated with ChIP-seq peaks using the default settings for the `annotatePeak` function in ChIPseeker v1.26.2 [25]. Gene domains for promoter- and enhancer- associated ChIP-seq peaks were used for gene ontology analysis. Gene ontology analysis was performed using clusterProfiler v4.1.4 [85], with Gene Ontology and KEGG annotation drawn from the `org.Mm.eg.db`

v3.12.0 database [86], setting an FDR-corrected p-value threshold of 0.05 for statistical significance. In order to use the mouse Ensembl GO annotations for the dunnart gene domains, we converted the Tasmanian devil RefSeq IDs to Ensembl v103 IDs using biomaRt v2.46.3 [87, 88], and then converted these to mouse Ensembl v103. In this way, we were able to assign Devil Ensembl IDs to 74% of genes with peaks, and mouse IDs to 95% of genes with a devil Ensembl ID. For calculating enrichment in GO and KEGG in the dunnart, the list of Tasmanian devil genes with an orthologous Ensembl gene in the mouse were used as the background list (Supplementary File).

Motif discovery and enrichment

Short sequence motifs enriched in dunnart promoter-associated peaks and enhancer-associated peaks were identified with Homer v4.11.1 [27] using `findMotifsGenome.pl`. In this case random GC- and length-match sequences for all promoters and enhancers were used as the background set to test for enrichment compared to random expectation. Enriched motifs were clustered into Homer motif families [27]. The full list of enriched motif families can be found in Supplementary File .

Mouse and dunnart peak comparison

Dunnart and mouse peaks called from normalised input reads were filtered to 50 bp regions centred on the peak summit. Dunnart peak coordinates were lifted over using liftOver [73] to the mouse (mm10) genome and then back to the dunnart genome. Alignable peaks were kept if after reciprocal liftOver they had the same nearest gene call. Alignable peaks were then intersected with enhancer- and promoter-associated peaks at each stage in the mouse bedtools intersect v.2.30.0 [84] to assess peaks with conserved activity.

RNA-seq timecourse clustering analysis

RNA-seq gene count tables for mouse embryonic facial prominence were downloaded from ENCODE (see Supplementary Table 10 for accession details). Genes were filtered to retain only those expressed at > 1 log CPM in both biological replicates at each of the developmental stages assayed. The resulting gene list was tested for differential expression with the `DBanalysis` function in TCseq package [30] which implements edgeR to fit read counts to a negative binomial generalised linear model (Supplementary File 4). Differentially expressed genes were described as genes with an absolute $\log_2$ fold-change > 2 compared to the starting time-point (E10.5) (Supplementary File 4). We then determined the optimal division of clusters using the Calinkski criterion implemented with the `cascadeKM` function in the vegan v. package [89] with the parameters: `inf.gr = 1, sup.g = 10 iter = 1000, criterion = "calinski"`. We ran the `timeclust` function with the parameters: `algo = 'cm', k = 5, standardize = TRUE` which performs unsupervised soft clustering of gene expression patterns into five clusters with similar z-scaled temporal patterns (Supplementary File).

Data availability

The data generated in this study have been deposited in NCBI's Gene Expression Omnibus [90, 91] and are available through GEO Series accession number GSE188990. To review GEO accession GSE188990: go to https://www.ncbi.nlm.nih.gov/geo/query/acc.cgi?acc=GSE188990 and enter token **kpgtqeqkvjgbtcd**. Accession IDs for previously published data sets from the ENCODE consortium [17, 28] are given in Supplementary Table 5. Processed data is available in figshare repository: https://figshare.com/account/home#/projects/140843. All analyses described were carried out using custom bash, Python3 and R v4.1.0 scripts, and are available at https://github.com/lecook/chipseq-cross-species.

References

1. Francis-West, P. & Crespo-Enriquez, I. *Vertebrate embryo: craniofacial development* **9** (John Wiley & Sons, Ltd, Chichester, UK, 2016).
2. Nunn, C. L. & Smith, K. K. Statistical analyses of developmental sequences: the craniofacial region in marsupial and placental mammals. *The American Naturalist* **152,** 82–101 (1998).
3. Smith, K. K. Craniofacial development in marsupial mammals: developmental origins of evolutionary change. *Developmental Dynamics* **235,** 1181–93 (2006).
4. Smith, K. K. The evolution of mammalian development. *Bulletin of the Museum of Comparative Zoology* **156,** 119–135 (2001).
5. Cook, L. E. *et al.* Postnatal development in a marsupial model, the fat-tailed dunnart (Sminthopsis crassicaudata; Dasyuromorphia: Dasyuridae). *Communications Biology* **4,** 1–14 (2021).
6. Smith, K. K. Comparative patterns of craniofacial development in eutherian and metatherian mammals. *Evolution* **51,** 1663–1678 (1997).
7. Spiekman, S. N. F. & Werneburg, I. Patterns in the bony skull development of marsupials: high variation in onset of ossification and conserved regions of bone contact. *Science Reports* **7,** 11 (2017).
8. Koyabu, D. *et al.* Mammalian skull heterochrony reveals modular evolution and a link between cranial development and brain size. *Nature Communications* **5,** 3625 (2014).
9. Goswami, A. *et al.* Do developmental constraints and high integration limit the evolution of the marsupial oral apparatus? *Integrative and Comparative Biology* **56,** 404–415 (2016).
10. Sears, K. E. Constraints on the morphological evolution of marsupial shoulder girdles. *Evolution* **58,** 2353–70 (2004).
11. Attanasio, C. *et al.* Fine tuning of craniofacial morphology by distant-acting developmental enhancers. *Science* **342,** 1241006 (2013).
12. Wakamatsu, Y. & Suzuki, K. Sequence alteration in the enhancer contributes to the heterochronic Sox9 expression in marsupial cranial neural crest. *Developmental Biology* **456,** 31–39 (2019).

13. Wakamatsu, Y. *et al.* Comparative gene expression analyses reveal heterochrony for Sox9 expression in the cranial neural crest during marsupial development. *Evolution & Development* **16,** 197–206 (2014).

14. Cook, L. E. *et al.* Postnatal development in a marsupial model, the fat-tailed dunnart (*Sminthopsis* crassicaudata; Dasyuromorphia: Dasuryidae). Morphosource repository. (2021).

15. Suarez, R. *et al.* Development of body, head and brain features in the australian fat-tailed dunnart (*Sminthopsis crassicaudata*; Marsupialia: Dasyuridae); A postnatal model of forebrain formation. *PLoS One* **12,** e0184450 (2017).

16. Visel, A. *et al.* VISTA enhancer browser–a database of tissue-specific human enhancers. *Nucleic Acids Research* **35,** D88–92 (2007).

17. ENCODE Project Consortium. An integrated encyclopedia of DNA elements in the human genome. *Nature* **489,** 57–74 (2012).

18. Villar, D. *et al.* Enhancer evolution across 20 mammalian species. *Cell* **160,** 554–566 (2015).

19. Heintzman, N. D. *et al.* Histone modifications at human enhancers reflect global cell-type-specific gene expression. *Nature* **459,** 108–112 (2009).

20. Zhu, J. *et al.* Genome-wide chromatin state transitions associated with developmental and environmental cues. *Cell* **152,** 642–654 (2013).

21. Cain, C. E. *et al.* Gene expression differences among primates are associated with changes in a histone epigenetic modification. *Genetics* **187,** 1225–1234 (2011).

22. Santos-Rosa, H. *et al.* Active genes are tri-methylated at k4 of histone h3. *Nature* **419,** 407–411 (2002).

23. Creyghton, M. P. *et al.* Histone H3K27ac separates active from poised enhancers and predicts developmental state. *Proceedings of the National Academy of Sciences of the United States of America* **107,** 21931–21936 (2010).

24. Kim, T.-K. *et al.* Widespread transcription at neuronal activity-regulated enhancers. *Nature* **465,** 182–187 (2010).

25. Yu, G. *et al.* ChIPseeker: an R/Bioconductor package for ChIP peak annotation, comparison and visualization. *Bioinformatics* **31,** 2382–2383 (2015).

26. Barski, A. *et al.* High-resolution profiling of histone methylations in the human genome. *Cell* **129,** 823–837 (2007).

27. Heinz, S. *et al.* Simple combinations of lineage-determining transcription factors prime cis-regulatory elements required for macrophage and B cell identities. *Molecular Cell* **38,** 576–589 (2010).

28. Davis, C. A. *et al.* The encyclopedia of DNA elements (ENCODE): data portal update. *Nucleic Acids Research* **46,** D794–D801 (D1 2018).

29. Lynch, M. *et al.* The repatterning of eukaryotic genomes by random genetic drift. *Annual Review of Genomics and Human Genetics* **12** (2011).

30. Wu, M. & Gu, L. *TCseq: time course sequencing data analysis* version 1.14.0. 2020.

31. Brinkley, J. F. *et al.* The FaceBase consortium: a comprehensive resource for craniofacial researchers. *Development* **143,** 2677–2688 (2016).

32. Smith, K. K. Early development of the neural plate, neural crest and facial region of marsupials. *Journal of Anatomy* **199,** 121–131 (2001).

33. Schneider, N. Y. & Gurovich, Y. Morphology and evolution of the oral shield in marsupial neonates including the newborn monito del monte (Dromiciops gliroides, Marsupialia Microbiotheria) pouch young. *Journal of Anatomy* **231,** 59–83 (2017).

34. Sánchez-Villagra, M. R. & Forasiepi, A. M. On the development of the chondrocranium and the histological anatomy of the head in perinatal stages of marsupial mammals. *Zoological Letters* **3,** 632 (2017).

35. Ferner, K. Skin structure in newborn marsupials with focus on cutaneous gas exchange. *Journal of Anatomy* **233,** 311–327 (2018).

36. Mess, A. M. & Ferner, K. J. Evolution and development of gas exchange structures in Mammalia: the placenta and the lung. *Respiratory Physiology & Neurobiology* **173,** S74–82 (2010).

37. Frappell, P. B. & MacFarlane, P. M. Development of the respiratory system in marsupials. *Respiratory Physiology & Neurobiology* **154,** 252–267 (2006).

38. Pralomkarn, T. *et al.* Postnatal development of the skin of the marsupial native cat *Dasyurus hallucatus*. *Journal of Morphology* **205,** 233–242 (1990).

39. Carelli, F. N. *et al.* Repurposing of promoters and enhancers during mammalian evolution. *Nature Communications* **9,** 4066 (2018).

40. Nord, A. S. *et al.* Rapid and pervasive changes in genome-wide enhancer usage during mammalian development. *Cell* **155,** 1521–1531 (2013).

41. Prescott, S. L. *et al.* Enhancer divergence and cis-regulatory evolution in the human and chimp neural crest. *Cell* **163,** 68–83 (2015).

42. Pointer, M. A. *et al.* RUNX2 tandem repeats and the evolution of facial length in placental mammals. *BMC evolutionary biology* **12,** 103 (2012).

43. Sears, K. E. *et al.* The correlated evolution of Runx2 tandem repeats, transcriptional activity, and facial length in carnivora. *Evolution & Development* **9,** 555–565 (2007).

44. Ritzman, T. B. *et al.* Facing the facts: The Runx2 gene is associated with variation in facial morphology in primates. *Journal of Human Evolution* **111,** 139–151 (2017).

45. Cleves, P. A. *et al.* Evolved tooth gain in sticklebacks is associated with a cis-regulatory allele of Bmp6. *Proceedings of the National Academy of Sciences of the United States of America* **111,** 13912–13917 (2014).

46. Cleves, P. A. *et al.* An intronic enhancer of Bmp6 underlies evolved tooth gain in sticklebacks. *PLoS genetics* **14,** e1007449 (2018).

47. Miller, C. T. *et al.* mef2ca is required in cranial neural crest to effect Endothelin1 signaling in zebrafish. *Developmental Biology* **308,** 144–157 (2007).

48. Jenkins, B. A. *et al.* The cellular basis of mechanosensory Merkel-cell innervation during development. *eLife* **8** (eds Nathans, J. & Bronner, M. E.) Publisher: eLife Sciences Publications, Ltd, e42633 (2019).

49. Fritzsch, B. An Integrated Perspective of Evolution and Development: From Genes to Function to Ear, Lateral Line and Electroreception. *Diversity* **13.** Number: 8 Publisher: Multidisciplinary Digital Publishing Institute, 364 (2021).

50. Li, L. *et al.* The Functional Organization of Cutaneous Low-Threshold Mechanosensory Neurons. *Cell* **147.** Publisher: Elsevier, 1615–1627 (2011).

51. Bai, L. *et al.* Genetic Identification of an Expansive Mechanoreceptor Sensitive to Skin Stroking. *Cell* **163.** Publisher: Elsevier, 1783–1795 (2015).

52. Desmarais, M. *et al.* Facial mechanosensory influence on forelimb movement in newborn opossums, *Monodelphis domestica*. *PLOS ONE* **11,** e0148352 (2016).

53. Gemmell, R. & Nelson, J. Ultrastructure of the olfactory system of three newborn marsupial species. *The Anatomical Record* **225,** 203–208 (1989).

54. Waite, P. M. *et al.* Timecourse of development of the wallaby trigeminal pathway. I. periphery to brainstem. *The Journal of Comparative Neurology* **350,** 75–95 (1994).

55. Jones, T. E. & Munger, B. L. Early differentiation of the afferent nervous system in glabrous snout skin of the opossum (*Monodelphis domesticus*). *Somatosensory Research* **3,** 169–184 (1985).

56. Shumate, A. & Salzberg, S. L. Liftoff: Accurate mapping of gene annotations. *Bioinformatics* **37,** 1639–1643 (2021).

57. (NHMRC), N. H.
bibinitperiod M. C. *Australian code for the care and use of animals for scientific purposes* (National Health and Medical Research Council, Canberra, 2013).

58. Bancroft, J. D. & Gamble, M. *Theory and practice of histological techniques* (Elsevier Health Sciences, 2008).

59. Schneider, C. A. *et al.* NIH image to ImageJ: 25 years of image analysis. *Nature Methods* **9,** 671–5 (2012).

60. Fishilevich, S. *et al.* GeneHancer: Genome-wide integration of enhancers and target genes in GeneCards. *Database* **2017,** 1217 (2017).

61. Sambrook, J. *et al. Molecular cloning: A laboratory manual.* (Cold Spring Harbor Laboratory Press, 1989).

62. Bolger, A. M. *et al.* Trimmomatic: A flexible trimmer for illumina sequence data. *Bioinformatics* **30,** 2114–2120 (2014).

63. Kolmogorov, M. *et al.* Assembly of long, error-prone reads using repeat graphs. *Nature Biotechnology* **37,** 540–546 (2019).

64. Pryszcz, L. P. & Gabaldón, T. Redundans: An assembly pipeline for highly heterozygous genomes. *Nucleic Acids Research* **44,** e113 (2016).

65. Walker, B. J. *et al.* Pilon: An integrated tool for comprehensive microbial variant detection and genome assembly improvement. *PLOS ONE* **9,** e112963 (2014).

66. Feigin, C. *et al.* A Chromosome-Scale Hybrid Genome Assembly of the Extinct Tasmanian Tiger (Thylacinus cynocephalus). *Genome Biology and Evolution* **14,** evac048 (2022).

67. Feigin, C. Y. *et al.* Genome of the Tasmanian tiger provides insights into the evolution and demography of an extinct marsupial carnivore. *Nature Ecology & Evolution* **2,** 182–192 (2018).

68. Renfree, M. B. *et al.* Genome sequence of an australian kangaroo, *Macropus eugenii*, provides insight into the evolution of mammalian reproduction and development. *Genome Biology* **12,** R81 (2011).

69. Murchison, E. P. *et al.* Genome sequencing and analysis of the Tasmanian devil and its transmissible cancer. *Cell* **148,** 780–791 (2012).

70. Mikkelsen, T. S. *et al.* Genome of the marsupial monodelphis domestica reveals innovation in non-coding sequences. *Nature* **447,** 167–177 (2007).

71. Peel, E. *et al.* A reference genome for the critically endangered woylie, Bettongia penicillata ogilbyi. *Gigabyte* **2021,** 1–15 (2021).

72. Brandies, P. A. *et al.* The first Antechinus reference genome provides a resource for investigating the genetic basis of semelparity and age-related neuropathologies. *Gigabyte* **2020,** 1–22 (2020).

73. Kent, W. J. *et al.* Evolution's cauldron: duplication, deletion, and rearrangement in the mouse and human genomes. *Proceedings of the National Academy of Sciences* **100,** 11484–11489 (2003).

74. Sharma, V. & Hiller, M. Increased alignment sensitivity improves the usage of genome alignments for comparative gene annotation. *Nucleic Acids Research* **45,** 8369–8377 (2017).

75. Suarez, H. G. *et al.* chainCleaner improves genome alignment specificity and sensitivity. *Bioinformatics* **33,** 1596–1603 (2017).

76. Dutheil, J. Y. *et al.* MafFilter: a highly flexible and extensible multiple genome alignment files processor. *BMC Genomics* **15,** 53 (2014).

77. Andrews, S. *FastQC: A quality control tool for high throughput sequence data [online]* 2010.

78. Martin, M. Cutadapt removes adapter sequences from high-throughput sequencing reads. *EMBnet.journal* **17,** 10–12 (2011).

79. Langmead, B. & Salzberg, S. L. Fast gapped-read alignment with Bowtie 2. *Nature methods* **9,** 357–359 (2012).

80. He, Y. *et al.* Spatiotemporal DNA methylome dynamics of the developing mouse fetus. *Nature* **583,** 752–759 (2020).

81. Li, H. *et al.* The Sequence Alignment/Map format and SAMtools. *Bioinformatics* **25,** 2078–2079 (2009).

82. Crusoe, M. R. *et al.* The khmer software package: enabling efficient nucleotide sequence analysis. *F1000Research* **4,** 900 (2015).

83. Zhang, Y. *et al.* Model-based analysis of ChIP-seq (MACS). *Genome Biology* **9,** R137 (2008).

84. Quinlan, A. R. & Hall, I. M. BEDTools: a flexible suite of utilities for comparing genomic features. *Bioinformatics* **26,** 841–842 (2010).

85. Wu, T. *et al.* clusterProfiler 4.0: A universal enrichment tool for interpreting omics data. *The Innovation* **2,** 100141 (2021).

86. Marc Carlson. *org.mm.eg.db: Genome wide annotation for mouse. R package version 3.12.0* 2020.

87. Durinck, S. *et al.* BioMart and Bioconductor: a powerful link between biological databases and microarray data analysis. *Bioinformatics (Oxford, England)* **21,** 3439–3440 (2005).

88. Durinck, S. *et al.* Mapping identifiers for the integration of genomic datasets with the R/Bioconductor package biomaRt. *Nature protocols* **4,** 1184–1191 (2009).

89. Jari Oksanen *et al. vegan: Community Ecology Package* version 2.5-7. 2020.

90. Barrett, T. *et al.* NCBI GEO: archive for functional genomics data sets—update. *Nucleic Acids Research* **41,** D991–D995 (2013).

91. Edgar, R. *et al.* Gene expression omnibus: NCBI gene expression and hybridization array data repository. *Nucleic Acids Research* **30,** 207–210 (2002).

92. Howe, K. L. *et al.* Ensembl 2021. *Nucleic Acids Research* **49,** D884–D891 (2021).

Acknowledgements

This research was supported by an Australian Government Research Training Program (RTP) Scholarship; the David Lachlan Hay Memorial Grant; Australian Research Council Grant (DP160103683)

Author contribution

L.E.C, I.G.R and A.J.P designed and conceived the study. L.E.C collected the tissue samples, performed the ChIP experiments, analysed the sequencing data and wrote the manuscript. C.Y.F performed the genome assembly and annotation. I.G.R and A.J.P supervised the study and gave editorial assistance. All authors reviewed and commented on the final manuscript.

List of Abbreviations

bp basepairs.

ChIP chromatin immunoprecipitation.

CPM counts per million mapped reads.

D postnatal day (in the fat-tailed dunnart).

DAPI 40,60-diamidino-2-phenylindole.

E embryonic day.

ENCODE encyclopedia of DNA elements.

FDR false discovery rate.

Gb gigabase pairs.

GO gene ontology.

H3K27ac acetylation of lysine residue at N-terminal position 27 of histone H3 protein.

H3K4me3 tri-methylation at 4th lysine residue of histone H3 protein.

IP immunoprecipitation.

kb kilobase pairs.

Mb megabase pairs.

NRF non-redundant fraction.

PWM position weight matrix.

qPCR quantitative PCR.

TF transcription factor.

TFBS transcription factor binding sites.

TSS transcription start site.

WGA whole genome alignment.